

Comparative Direct Analysis of Type Ia Supernova Spectra. I. SN 1994D

David Branch, E. Baron, Nicholas Hall, Mercy Melakayil, & Jerod Parrent

*Department of Physics and Astronomy, University of Oklahoma, Norman, Oklahoma
73019, USA; e-mail: branch@nhn.ou.edu*

ABSTRACT

As the first step in a comprehensive, comparative, direct analysis of the spectra of Type Ia supernovae (SNe Ia), we use the parameterized supernova synthetic-spectrum code, **Synow**, to interpret 26 spectra of the well-observed SN 1994D. Our results are consistent with the traditional view that the composition structure (element abundance fractions versus ejection velocity) is radially stratified. We find that resonance-scattering features due to permitted lines of Ca II, Na I, and Fe II persist to more than 100 days after explosion. The fitting parameters for SN 1994D, together with those to be determined for other SNe Ia, will provide an internally consistent quantification of the spectroscopic diversity among SNe Ia, and shed light on how the various manifestations of observational diversity are related to their physical causes.

Subject headings: supernovae: general – supernovae: individual (SN 1994D)

1. INTRODUCTION

This is the first in a series of articles on a comprehensive, comparative, direct analysis of spectra of Type Ia supernovae (SNe Ia). We are using the parameterized resonance-scattering synthetic-spectrum code **Synow** to fit all of the SN Ia spectra (other than very late-time spectra) that are available to us. Our motivations include the following. First, the process of extracting information from supernova spectra begins with line identifications, but the identifications of some SN Ia spectral features remain uncertain, and conflicting identifications can be found in the literature. We hope to improve this situation. Second, we will generate an ensemble of **Synow** fitting parameters that will provide an internally consistent quantification of the spectroscopic differences among SNe Ia. This should lead to an improved understanding of how the various manifestations of SN Ia diversity are related to their physical causes.

This article is concerned only with SN 1994D, a well observed, spectroscopically normal SN Ia that will serve as a standard of comparison for our analyses of other SN Ia spectra. In forthcoming articles we will present results for normal SNe Ia, and then for peculiar SNe Ia.

In this article we confine our attention to optical spectra, from the Ca II H&K blend (gf -weighted rest wavelength $\lambda 3945$) in the blue to the Ca II infrared triplet (Ca II IR3; gf -weighted rest wavelength $\lambda 8579$) in the red. The 26 spectra selected for study (Table 1) include 15 from Patat et al. (1996), 8 from Filippenko (1997), and 3 from Meikle et al. (1996). They range from 12 days before to 115 days after the date of maximum light in the B band, 1994 March 21. (We also will comment on a spectrum obtained 283 days after maximum light.) All spectra have been corrected for the 448 km s^{-1} redshift of the parent-galaxy, NGC 4526, but not for interstellar reddening, which is believed to be small.

2. CALCULATIONS

The elements of line formation in supernova spectra have been discussed and illustrated by Jeffery & Branch (1990) and Branch, Baron & Jeffery (2003), and will not be repeated here. The **Synow** code is based on simple assumptions: spherical symmetry; homologous expansion ($v = r/t$); a sharp photosphere that emits a blackbody continuous spectrum; and line formation by resonance scattering, treated in the Sobolev approximation. A synthetic spectrum consists of blended P Cygni profiles (unshifted emission component, blueshifted absorption component) superimposed on a continuum. **Synow** does not do continuum transport, it does not solve rate equations, and it does not calculate ionization ratios. Its main function is to take line multiple scattering into account so that it can be used in an empirical spirit to make line identifications and estimate the velocity at the photosphere (or pseudo-photosphere) and the velocity interval within which each ion is detected. These quantities provide constraints on the composition structure of the ejected matter.

For each ion that is introduced, the optical depth of a reference line at one velocity (ordinarily the velocity at the photosphere) is a fitting parameter and the optical depths of the other lines of the ion at that velocity are calculated assuming Boltzmann excitation at temperature T_{exc} . In this article, to keep the number of fitting parameters under control, T_{exc} is taken to have the same value for all ions at a given epoch: 10,000 K at premaximum and near-maximum epochs and 7000 K for postmaximum epochs. All line optical depths are taken to decrease exponentially with velocity, with e-folding velocity v_e usually taken to be 1000 km s^{-1} . At each epoch, the important fitting parameters are the velocity at the photosphere, v_{phot} , the optical depths of the ion reference lines, and whatever minimum and maximum velocities may be imposed on individual ions. When a minimum velocity is

imposed that exceeds the velocity at the photosphere, the ion is said to be detached (from the photosphere) at that minimum velocity. The temperature of the blackbody continuum T_{bb} is chosen to fit the overall slope of the spectrum; its value has limited physical significance because (1) the true continuum (or quasi-continuum) is not Planckian and (2) interstellar extinction and wavelength-dependent errors in the observed spectrum can affect the best fitting value of T_{bb} .

3. COMPARISONS

3.1. Near Maximum Light

We begin with the spectrum that is nearest to maximum light, at day -1 . In Figure 1 it is compared with a synthetic spectrum that has $v_{phot} = 11,000 \text{ km s}^{-1}$, $T_{bb} = 13,000 \text{ K}$, and includes lines of ten ions: O I, Na I, Mg II, Si II, Si III, S II, Ca II, Fe III, Co II, and Ni II. A value of $v_e = 1000 \text{ km s}^{-1}$ is used for all ions. Ions responsible for absorption features in the synthetic spectrum are labelled. Optical depths of the reference lines are in Table 1. Note that in addition to its photospheric component, Ca II has a high-velocity component, detached at $19,000 \text{ km s}^{-1}$. Detached high-velocity calcium in SN Ia spectra was first identified by Hatano et al. (1999a; in SN 1994D) and has been discussed by Wang et al. (2003; in SN 2001el), Thomas et al. (2004; in SN 2000cx) Gerardy et al. (2004; in SN 2003du), and Mazzali et al. (2004; in SN 1999ee). We are confident of the presence in the observed spectrum of O I (here slightly detached at $12,000 \text{ km s}^{-1}$), Mg II, Si II, Si III, S II, Ca II (both photospheric and high-velocity), and Fe III. The presence in the observed spectrum of Na I, Co II, and Ni II is not definite, but we use their lines in the synthetic spectrum because the Na I D lines improve the fit to the observed absorption near 5770 \AA , Co II lines improve the fit to the observed absorption near 4020 \AA , and Ni II lines lower what otherwise would be an excessively high Ca II H&K emission peak.

On the whole the fit is good, by supernova standards, although there are discrepancies. The optical depths of the Ca II photospheric and high-velocity components are chosen to fit the observed Ca II IR3 features because, being weaker than Ca II H&K, they are more sensitive to optical depth; this results in the synthetic Ca II H&K absorptions (both photospheric and high-velocity) being too deep. The discrepancy around the 5770 \AA absorption has been encountered in previous work with **Synow**. Lines of S II may be responsible for the observed absorptions at 4670 \AA and 4770 \AA , but the synthetic S II absorptions are too weak and too blueshifted. (Lines of high-velocity detached Fe II, not used in this synthetic spectrum but definitely needed at earlier epochs (§3.2), may also contribute to these two observed absorptions.) The synthetic O I feature is superimposed on a continuum which, as

we have seen in previous **Synow** work, is too high, owing to our use of a blackbody continuum. Additional ions would need to be introduced to beat down the synthetic spectrum at wavelengths shorter than the Ca II H&K absorption.

3.2. Premaximum

Figure 2 shows ten premaximum spectra, including the day -1 spectrum discussed in §3.1. Vertical dashed lines, drawn to guide the eye, refer to Ca II $\lambda 3945$ blueshifted by $20,000 \text{ km s}^{-1}$, Si II $\lambda 6355$ blueshifted by $10,000 \text{ km s}^{-1}$, and Ca II IR3 blueshifted by $20,000 \text{ km s}^{-1}$. Between day -1 and day -9 the spectra change slowly; between day -9 and day -12 the evolution is more rapid.

In Figure 3 the day -9 spectrum is compared with a synthetic spectrum that has $v_{phot} = 13,000 \text{ km s}^{-1}$, $T_{bb} = 12,000 \text{ K}$, and includes lines of ten ions: C II, high-velocity Fe II detached at $20,000 \text{ km s}^{-1}$, and the ions used for the day -1 spectrum except for Co II and Ni II. In the synthetic spectrum both Ca II and O I have detached high-velocity components. For some of the ions a value of v_e other than 1000 km s^{-1} is used to improve the fit, but the v_e values are not well determined. The fit is good and all discrepancies are mild. We are confident of the presence in the observed spectrum of O I (photospheric), Mg II, Si II, Si III, S II, Ca II (both photospheric and high-velocity), Fe III, and high-velocity Fe II. Based on the spectra of SN 1994D alone, the case for the presence of C II lines might not be convincing, but since we are confident of their presence in early spectra of some other SNe Ia, (e.g., SN 1998aq; Branch et al. 2003), and they do improve the fits for SN 1994D, we believe that they are present in SN 1994D. The spectroscopic case for detached high-velocity O I, based on one weak feature, is not compelling, but the possibility of detecting it has been discussed by Gerardy et al. (2004) and including it does improve the fit. The high-velocity Fe II lines are discussed below, where the need for them is more clear.

In Figure 4 the day -12 spectrum is compared with a synthetic spectrum that has $v_{phot} = 14,000 \text{ km s}^{-1}$, $T_{bb} = 11,000 \text{ K}$, and includes lines of eight ions: the same ones used for day -9 except for Mg II and Fe III. At this epoch we use $v_e = 2000 \text{ km s}^{-1}$ for most ions. The fit is good although there are several discrepancies. We are confident of all identifications given in Figure 4, except for Na I. Because the observed spectrum does not extend to Ca II IR3, and the Ca II H&K feature is so broad and deep that the photospheric and detached components are badly blended, the fitting parameters for the photospheric and detached Ca II components are very poorly constrained.

Detached high-velocity Fe II in early SN Ia spectra was first suggested by Hatano et al.

(1999a), on the basis of this day -12 spectrum of SN 1994D, and it has been discussed by Branch et al. (2003; in SN 1998aq) and Mazzali et al. (2005; in SN 1999ee). These lines have a strong influence on our synthetic spectrum of Figure 4. The long-dashed line shows the effects of removing them. Note that in the full synthetic spectrum the S II absorptions appear to be weak, while in the synthetic spectrum without the high-velocity Fe II lines they appear stronger, even though their optical depths have not changed. This means that their apparent weakness in the full synthetic spectrum, and in the observed spectrum, is not because of a lack of optical depth in the S II lines, but because they are partially filled in by the P-Cygni emission components of high-velocity Fe II lines.

Reference-line optical depths for all of our premaximum fits, including those that are not displayed in figures, are listed in Table 1. A blank entry, such as for O I at day -11 , is used when the wavelength coverage is such that an ion that might be expected to be present, based on previous or subsequent spectra, cannot be seen. The large changes in the photospheric and detached Ca II optical depths from day -10 to day -9 are a consequence of only the H&K feature being covered in the former spectrum and only the IR3 feature in the latter.

Before leaving the premaximum phase we should mention that the day -10 and day -11 spectra contain a weak absorption feature near 6630 \AA that has a full width of only 270 km s^{-1} . The feature apparently is real (F. Patat, personal communication). We are unable to suggest a plausible identification. It probably is not He I $\lambda 6678$ because there is no corresponding feature that could be attributed to $\lambda 5876$, which should be stronger. An absorption feature due to $H\alpha$, redshifted by 3000 km s^{-1} and therefore implying infall, also seems unlikely. Similar features should be sought in spectra of other SNe Ia.

3.3. The Postmaximum Si II Phase

Figure 5 shows eight observed spectra, from day -1 (repeated from Figure 2) to day $+12$. We refer to the interval from day $+2$ to day $+12$ as the postmaximum Si II phase because the 6130 \AA absorption is deep and apparently unblended, at least in its core. The wavelength of the absorption minimum hardly changes during this phase. The S II features gradually disappear; they are still visible (barely) at day $+11$, but not at day $+12$. The absorption observed at 5770 \AA on day -1 shifts blueward to 5690 \AA by day $+12$ and develops an extended blue wing. We attribute this to strengthening of the Na I D lines. The gradual changes at wavelengths shorter than 5200 \AA are due to the fading of Mg II, Si III, and Fe III and the development of Co II and Fe II (see the reference-line optical depths in Table 1).

Figure 6 compares the day +12 spectrum with a synthetic spectrum that has $v_{phot} = 10,000 \text{ km s}^{-1}$, $T_{bb} = 12,000 \text{ K}$, and includes lines of eight ions: O I, Na I, Si II, Ca II, Cr II, Fe II, Co II, and Ni II. We use $v_e = 1000 \text{ km s}^{-1}$ for most ions, although 3000 km s^{-1} is used for Na I. The fit is not bad except for the severe problem from 6600 \AA to 8100 \AA . Between the Ca II H&K and Na I features the synthetic spectrum is a complex blend of many lines: mainly Co II and Fe II, with some contributions from Cr II. In the observed spectrum the 6130 \AA Si II absorption is beginning to be flanked by weak Fe II features (see §3.4) that are too weak in the synthetic spectrum.

3.4. The Si II–to–Fe II Transition Phase

At this point we switch from plotting flux per unit frequency interval to flux per unit wavelength interval, because the spectra are becoming redder and flux per unit wavelength interval makes the spectra look flatter and easier to inspect. Figure 7 shows seven observed spectra, from day +12 (repeated from Figure 5) to day +28. We refer to the interval from day +14 to day +28 as the Si II–to–Fe II transition phase. At day +14 the core of the deep red Si II absorption begins to appear blended on its red side. At day +28 the very core of the Si II absorption is still present, but strongly blended on both sides, due to the strengthening of Fe II lines. During this phase a striking spectral evolution occurs in the 5200 \AA to 5600 \AA region. As a weak absorption at 5350 \AA strengthens, the ratio of the flanking emission peaks evolves very strongly, from slightly higher on the left side of the absorption at day +14 to much higher on the right side at day +28. Our fits nicely account for this evolution in terms of strengthening Fe II and Cr II lines.

Figure 8 compares the day +28 spectrum with a synthetic spectrum that has $v_{phot} = 9000 \text{ km s}^{-1}$, $T_{bb} = 7500 \text{ K}$, and includes lines of six ions: Na I, Si II, Ca II, Cr II, Fe II, and Co II. At this and other epochs from day 14 to day 115, the imposition of a maximum velocity of $13,000 \text{ km s}^{-1}$ on Cr II, Fe II, and Co II improves the fit. Note that the two flux peaks that flank the 5350 \AA absorption, mentioned in the previous paragraph, are well matched. The spectrum between the Ca II H&K and Na I features remains a complex blend of many lines, but now mainly Fe II, with some contributions from Co II and Cr II. We believe that the line identifications in Figure 8 are correct as far as they go, but we have not found a plausible way to remove the discrepancy to the right of the 6500 \AA flux peak.

3.5. The Fe II Phase

Figure 9 shows five observed spectra, from day +28 (repeated from Figure 7) to day +283. We refer to the interval from day +50 to day +115 as the Fe II phase, because the Si II line is all but gone (in our synthetic spectrum for day 50, Si II detached at 9000 km s^{-1} still has a small effect) and apart from the persistent Ca II and Na I features the spectrum is mainly shaped by Fe II lines. Most of the spectral features retain their identities and evolve slowly during this phase, although the Na I feature becomes much stronger, and an apparent emission peak develops at 7370 \AA . The day +50 spectrum can be fit about as well as the day +28 spectrum (Figure 8), in much the same way.

Figure 10 compares the day +115 spectrum with a synthetic spectrum that has $v_{phot} = 6000 \text{ km s}^{-1}$, $T_{bb} = 15,000 \text{ K}$, and includes lines of only four ions: Na I, Ca II, Fe II, and Co II. The high value of T_{bb} was chosen on the basis of wavelengths longer than 4500 \AA ; this leaves the synthetic spectrum much too high at wavelengths shorter than 4400 \AA . The discrepancy may be due to a strong departure from an underlying blackbody continuum, and to severe underblanketing in the synthetic spectrum. (Lines of neutral iron-group elements may help to blanket the observed spectrum at this epoch; see Pastorello et al. (2004) on the spectrum of the Type II SN 1998A.) The synthetic spectrum also fails completely from 6600 \AA to 7600 \AA . Nevertheless, the fit from 4500 \AA to 6500 \AA , although not good, is sufficient to suggest that, contrary to what is usually assumed, the spectrum at 100 days postmaximum is not just a blend of forbidden emission lines — it is largely shaped by permitted Fe II lines, especially in the blue.

The overall shape of the day +283 spectrum (Figure 9) differs from that of the day +115 spectrum, and the assumption of an underlying blackbody continuum at day +283 would be completely untenable, yet most of the flux minima are at practically the same wavelengths in these two spectra. If the day +283 spectrum consisted just of forbidden emission lines, with no absorption features, these similarities would be strangely coincidental. However, Ca II H&K absorption is apparent in the day +283 spectrum, and Ca II IR3 and Na I absorptions appear to be present as well. In addition, the sharp absorption at 4100 \AA may be produced by Ca I $\lambda 4226$ (a resonance line), blueshifted by 8900 km s^{-1} . The extent to which SN Ia spectra as late as day +283 are affected by Fe II permitted lines, as well, will be addressed in a future article, when we have the opportunity to study spectra in the interval between day +115 and day +283.

4. DISCUSSION

We have been able to identify nearly all of the spectral features of SN 1994D with lines of plausible ions — mostly in the same way they have been identified in spectra of normal SNe Ia before (e.g., Branch et al. 1983; Jeffery et al. 1992; Kirshner et al. 1993; Mazzali et al. 1993; Branch et al. 2003). Our fits to all but the latest spectra are satisfactory, considering the approximations made, which include spherical symmetry. Qualitatively, our results are consistent with the traditional view that the SN Ia composition structure is strongly radially stratified (Figure 11), e.g., C II only above 13,000 km s⁻¹ and O I only above 12,000 km s⁻¹.

The reference-line optical depths of Table 1 could be used, together with LTE line-optical-depth calculations such as those of Hatano et al. (1999b), to estimate element abundance ratios, but these would be subject to serious uncertainties. In general, quantitative inferences about element abundances should be made by means of detailed spectrum calculations for nuclear-hydrodynamical explosion models that include complete composition structures (e.g., Höflich 1995 and Lentz et al. 2001 for SN 1994D). However, a few of the quantitative implications of our present results should be mentioned. Since we have invoked the presence of permitted Fe II, Ca II, and Na I features at relatively late times, we make rough estimates of the amount of mass in these ionization states that would be needed to produce the optical depths. For a given ionization stage, the amount of mass required to fill a uniform-density sphere of radius vt at time t after explosion is

$$M(\text{ion})/M_{\odot} \simeq 10^{-14} v_4^3 t_d^2 A \tau/f \lambda_{\mu} x_{\ell},$$

where v_4 is in units of 10⁴ km s⁻¹, t_d is in days, A is atomic weight, f is oscillator strength, λ_{μ} is in microns, and x_{ℓ} is the fraction of the ion population in the lower level of the transition. With $v_4 = 0.6$ and $t_d = 100$, the amount of singly ionized iron required to produce a reference-line optical depth of 50 is about 0.01 M_{\odot} . The amount of singly ionized calcium required to produce a reference-line optical depth of 10⁴ is about $4 \times 10^{-4} M_{\odot}$. (For comparison, the total amount of calcium in the sun is $6.4 \times 10^{-5} M_{\odot}$.) The amount of neutral sodium required to produce a reference-line optical depth of 10 is $3 \times 10^{-7} M_{\odot}$. (The total amount of sodium in the sun is $3.4 \times 10^{-5} M_{\odot}$.) These mass requirements are modest, provided that the fractions of singly ionized iron, singly ionized calcium, and neutral sodium, are not extremely small.

The relative optical depths of Ni II, Co II, and Fe II, and of Ni III, Co III, and Fe III, do not depend critically on temperature and electron density, therefore we ask whether the relative optical depths that we have used for these ions appear to be reasonable, on the basis of LTE line optical depth calculations. Briefly, we find the following: (1) The iron

responsible for the detached high-velocity features at early times was not formed from the decay of ^{56}Ni through ^{56}Co , otherwise Ni II and Co II lines would be too strong. (2) There is no conflict between the presence of Fe III lines and the absence of Co III and Ni III lines from day -4 to day 7. (3) The ratios of the postmaximum Co II and Fe II optical depths are roughly consistent with cobalt and iron both having been formed from ^{56}Ni decay (or, more reasonably, with small amounts of directly synthesized iron, cobalt, and nickel such that their final relative abundances match their relative abundances in the sun). (4) If the Ni II identifications from day 10 to day 17 are correct, then the nickel responsible for these features cannot have been formed as ^{56}Ni , but must have been synthesized directly, as stable ^{58}Ni .

The optical depths listed in Table 1 indicate which ions are responsible for shaping the spectrum of SN 1994D at each epoch. The main utility of these parameters, however, will be to serve as a standard of comparison for other SNe Ia.

We are grateful to Nando Patat, Alex Filippenko, and Peter Meikle for providing spectra, and to David Jeffery and Jason Zinn for assistance. This work has been supported by NSF grant AST-0204771 and NASA LTSA grant NNG04GD36G.

REFERENCES

- Branch, D., Baron, E., & Jeffery, D. J. 2003, in *Supernovae and Gamma-Ray Bursters*, ed. K. Weiler (Heidelberg: Springer), 47
- Branch, D., Lacy, M. L., McCall, M. L., Sutherland, P. G., Uomoto, A., Wheeler, J. C., & Wills, B. J. 1983, *ApJ*, 270, 123
- Branch, D., et al. 2003, *AJ*, 126, 1489
- Filippenko, A. V. 1997, in *Thermonuclear Supernovae*, eds. P. Ruiz-Lapiente, R. Canal, & J. Isern (Dordrecht: Kluwer), 1
- Gerardy, C. L., et al. 2004, *ApJ*, 607, 391
- Hatano, K., Branch, D., Fisher, A., Baron, E., & Filippenko, A. V. 1999a, *ApJ*, 525, 881
- Hatano, K., Branch, D., Fisher, A., Millard, J., & Baron, E. 1999b, *ApJS*, 121, 233
- Höflich, P. 1995, *ApJ*, 443, 89
- Jeffery, D. J. & Branch, D. 1990, in *Supernovae*, eds. J. C. Wheeler, T. Piran, & S. Weinberg (Singapore: World Scientific). 149
- Jeffery, D. J., Leibundgut, B., Kirshner, R. P., Benetti, S., Branch, D., & Sonneborn, G. 1992, *ApJ*, 397, 304
- Kirshner, R. P., et al. 1993, *ApJ*, 415, 589
- Lentz, E. J., Baron, E., Branch, D., & Hauschildt, P. H. 2001, *ApJ*, 557, 266
- Mazzali, P. A., et al. 2005, *MNRAS*, 357, 200
- Mazzali, P. A., Lucy, L. B., Danziger, I. J., Gouiffes, C., Cappellaro, E., & Turatto, M. 1993, *A&A*, 269, 423
- Meikle, W. P. S., et al. 1996, *MNRAS*, 281, 263
- Pastorello, A., et al. 2004, *MNRAS*, in press
- Patat, F., Benetti, S., Cappellaro, E., Danziger, I. J., Della Valle, M., Mazzali, P. A., & Turatto, M. 1996, *MNRAS*, 278, 111
- Thomas, R. C., Branch, D., Nomoto, K., Li, W., & Filippenko, A. V. 2004, *ApJ*, 601, 1019
- Wang, L., et al. 2003, *ApJ*, 591, 1110

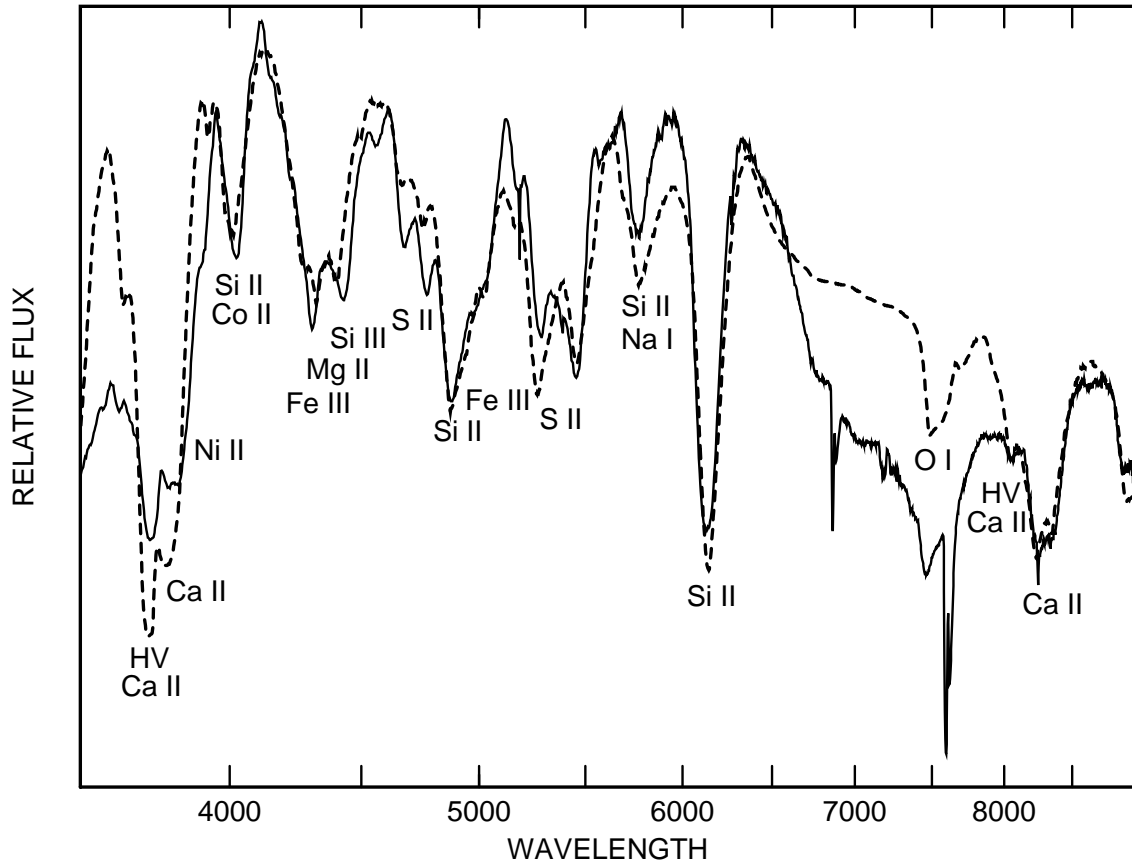


Fig. 1.— The day -1 spectrum of SN 1994D (*solid line*) is compared with a synthetic spectrum (*dashed line*) that has $v_{phot} = 11,000 \text{ km s}^{-1}$, $T_{bb} = 13,000 \text{ K}$, and includes lines of ten ions. The flux is per unit frequency interval.

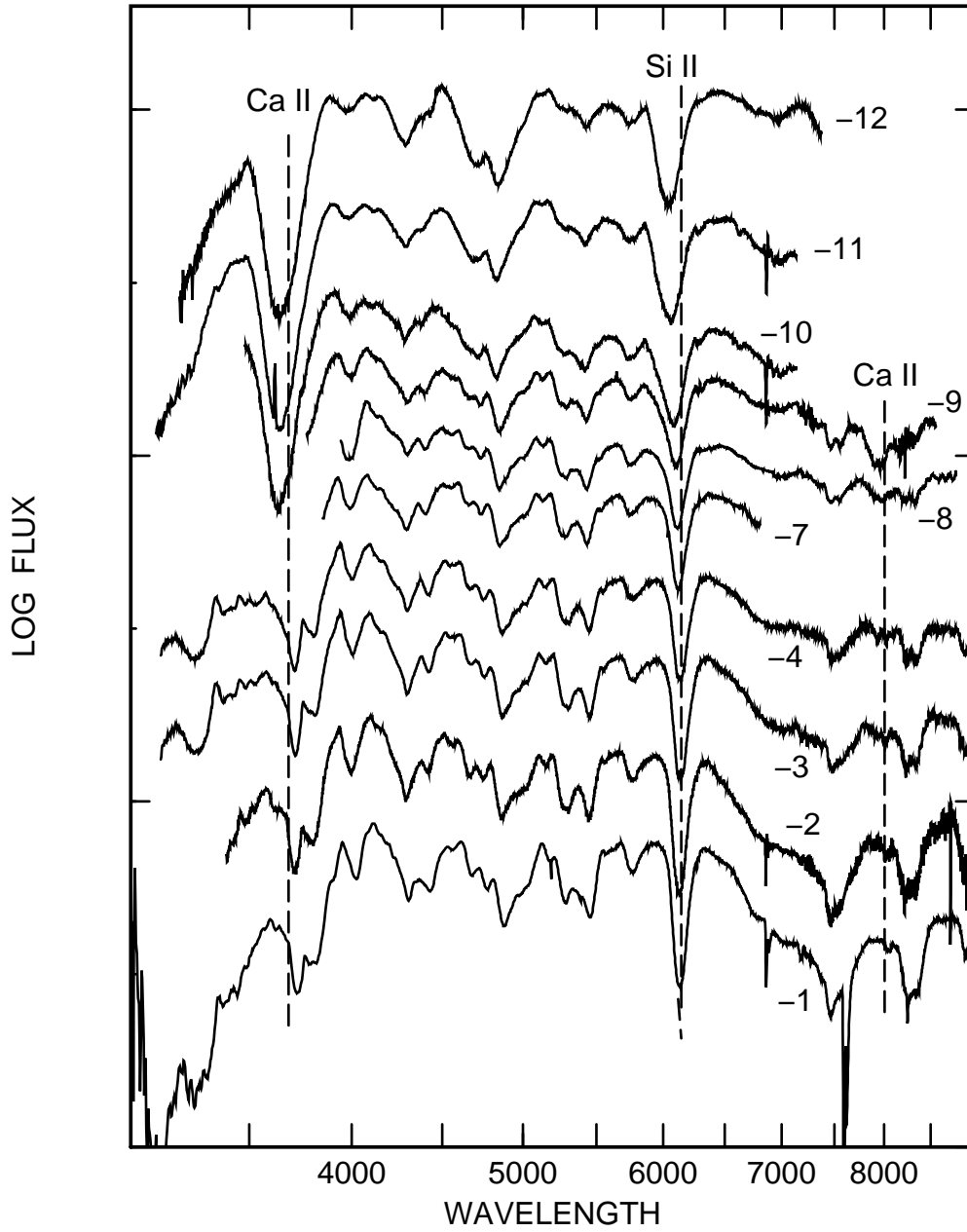


Fig. 2.— Ten spectra of SN 1994D. Epochs are in days with respect to the date of maximum brightness in the *B* band. The flux is per unit frequency interval and the vertical displacement is arbitrary. Vertical dashed lines refer to Ca II λ 3945 blueshifted by $20,000 \text{ km s}^{-1}$, Si II λ 6355 blueshifted by $10,000 \text{ km s}^{-1}$, and Ca II IR3 blueshifted by $20,000 \text{ km s}^{-1}$.

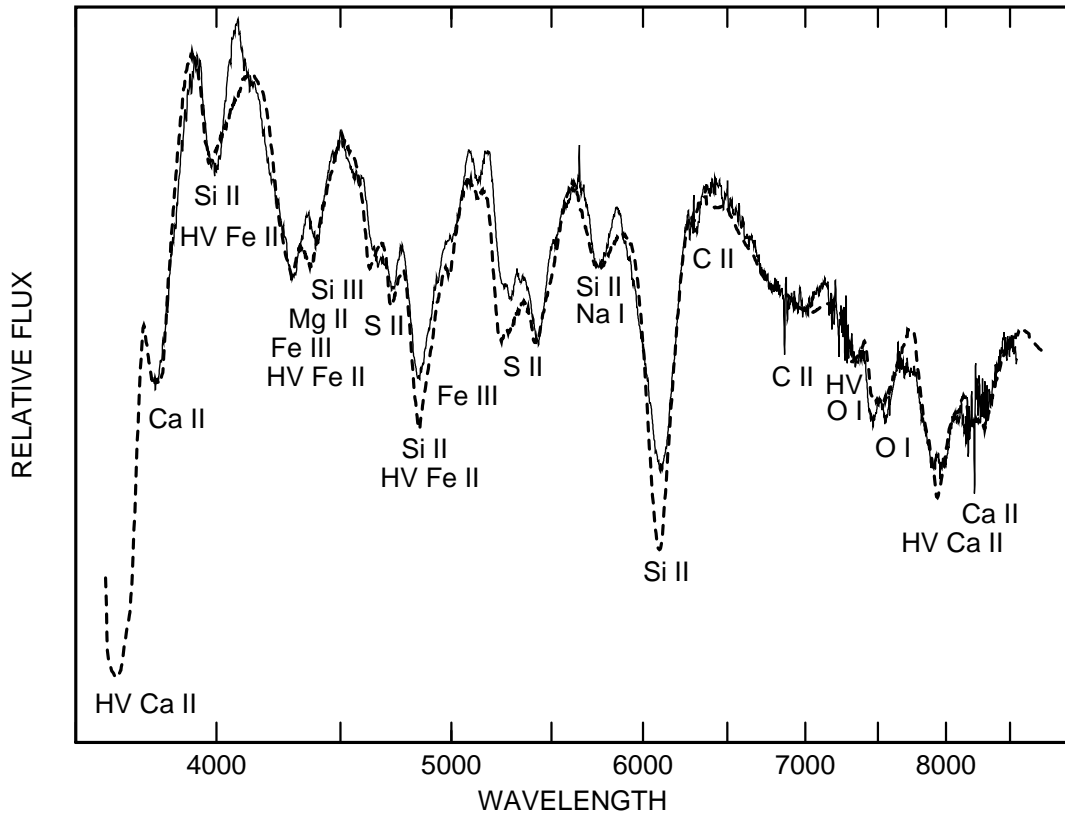


Fig. 3.— The day -9 spectrum of SN 1994D (*solid line*) is compared with a synthetic spectrum (*dashed line*) that has $v_{phot} = 13,000 \text{ km s}^{-1}$, $T_{bb} = 12,000 \text{ K}$, and includes lines of ten ions. The flux is per unit frequency interval.

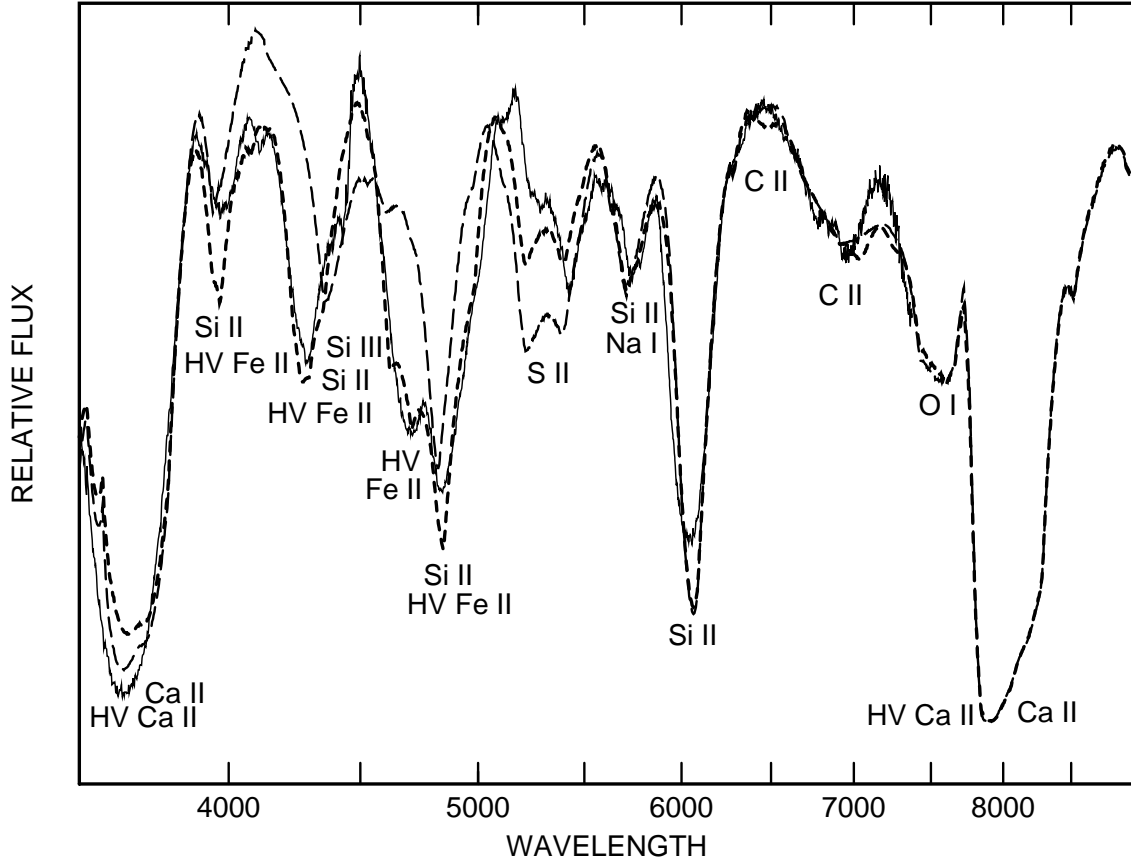


Fig. 4.— The day -12 spectrum of SN 1994D (*solid line*) is compared with a synthetic spectrum (*short-dashed line*) that has $v_{phot} = 14,000 \text{ km s}^{-1}$, $T_{bb} = 11,000 \text{ K}$, and includes lines of eight ions, and with the same synthetic spectrum without the high-velocity Fe II lines (*long-dashed line*). The flux is per unit frequency interval.

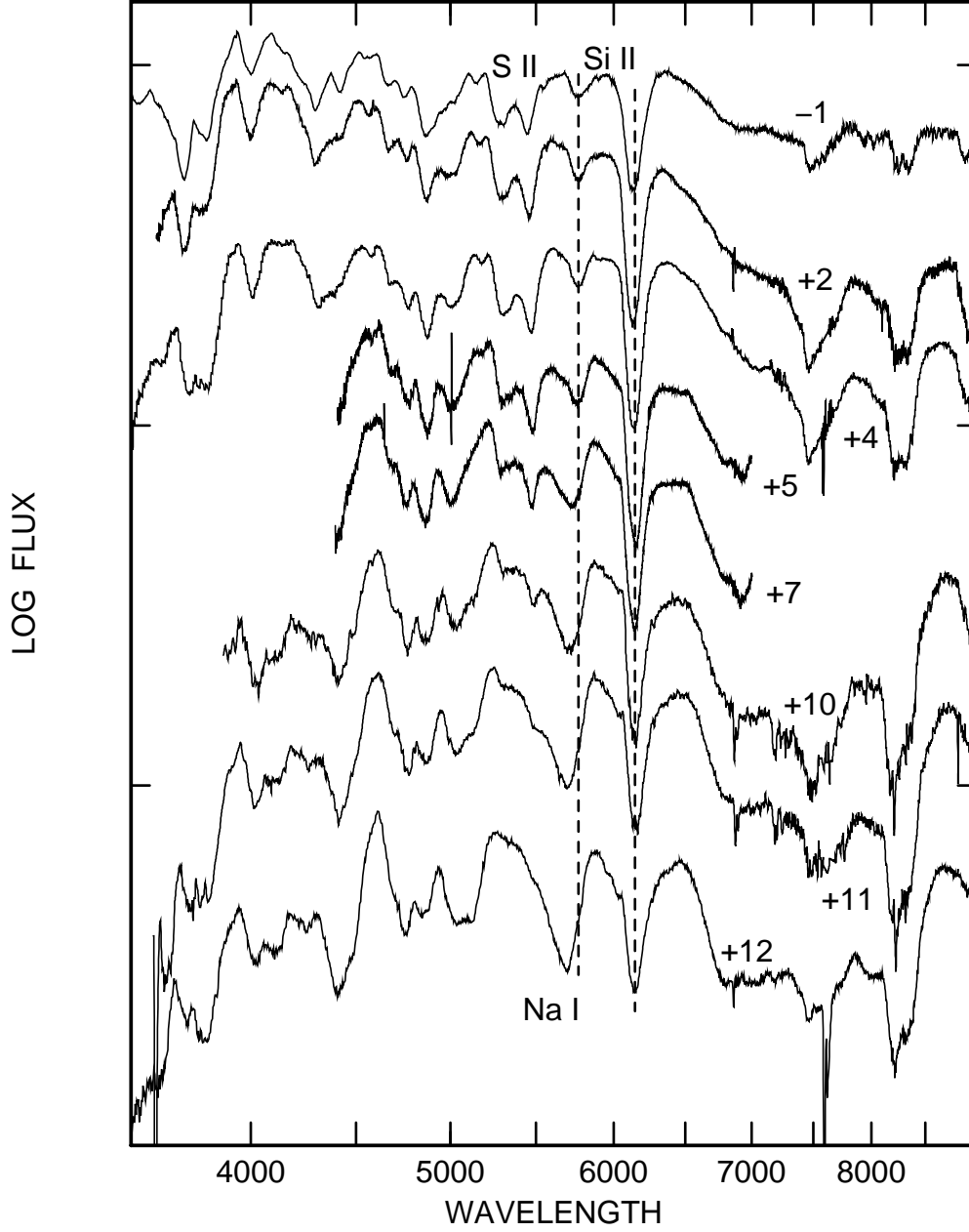


Fig. 5.— Eight spectra of SN 1994D. The flux is per unit frequency interval. Vertical dashed lines refer to Si II $\lambda 5972$ and $\lambda 6355$, both blueshifted by $10,000 \text{ km s}^{-1}$.

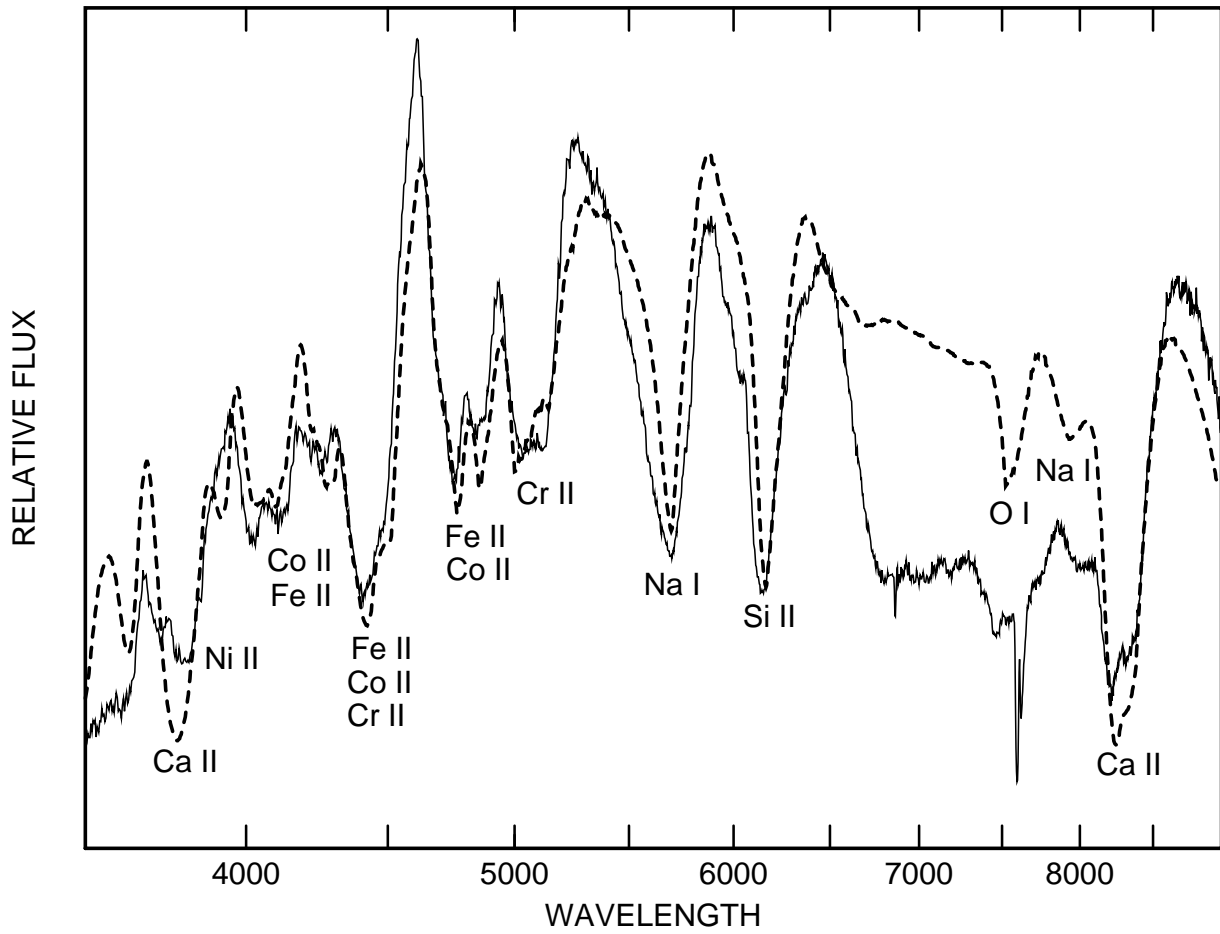


Fig. 6.— The day +12 spectrum of SN 1994D (*solid line*) is compared with a synthetic spectrum (*dashed line*) that has $v_{phot} = 10,000 \text{ km s}^{-1}$, $T_{bb} = 12,000 \text{ K}$, and includes lines of eight ions. The flux is per unit frequency interval.

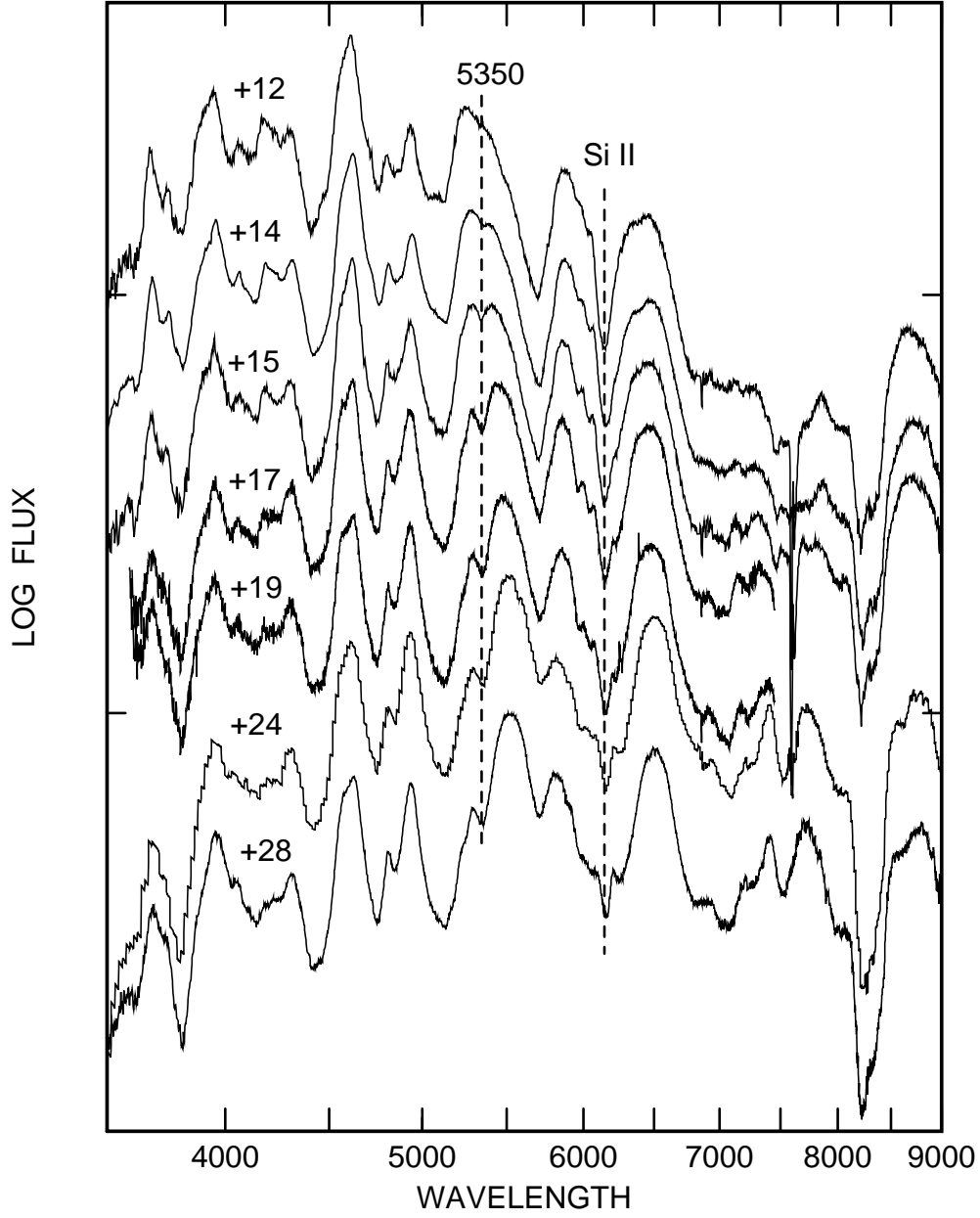


Fig. 7.— Seven spectra of SN 1994D. The flux is per unit wavelength interval. One vertical dashed line is at 5350 Å and the other refers to Si II λ 6355 blueshifted by 10,000 km s⁻¹.

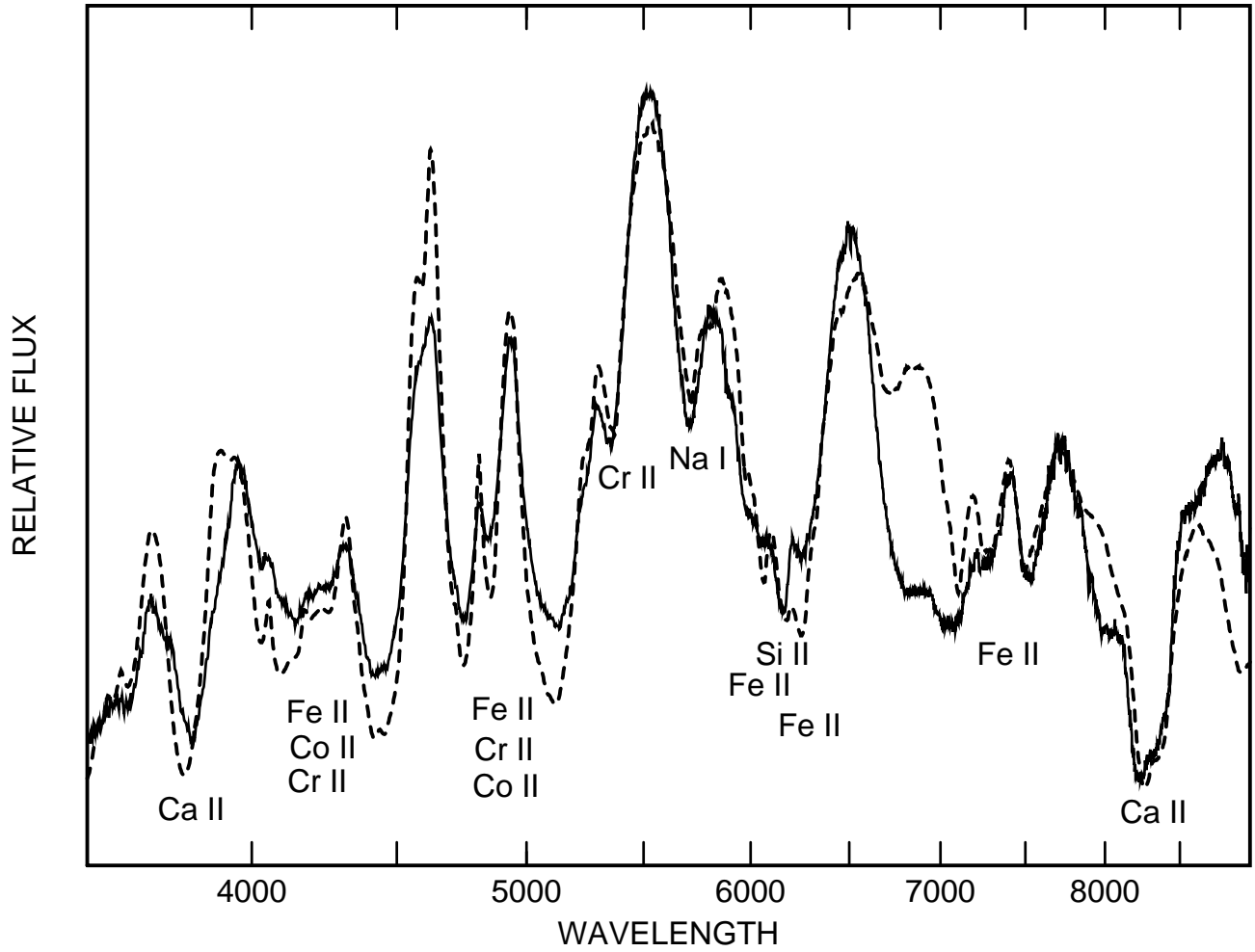


Fig. 8.— The day +28 spectrum of SN 1994D (*solid line*) is compared with a synthetic spectrum (*dashed line*) that has $v_{phot} = 9000 \text{ km s}^{-1}$, $T_{bb} = 7500 \text{ K}$, and contains lines of six ions. The flux is per unit wavelength interval.

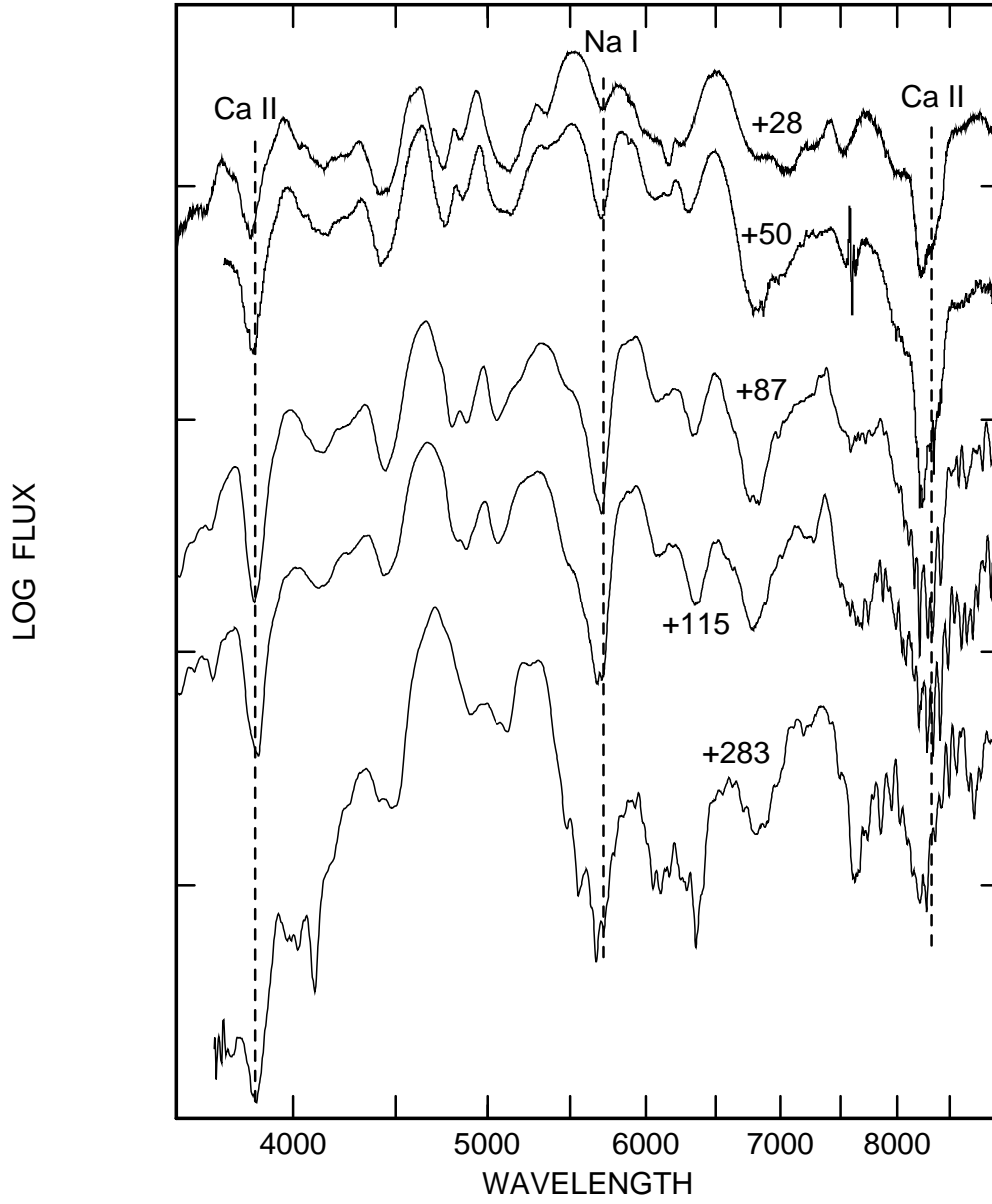


Fig. 9.— Five spectra of SN 1994D. The flux is per unit wavelength interval. Vertical dashed lines refer to Ca II λ 3945, Na I λ 5892, and Ca II IR3, each blueshifted by 9000 km s^{-1} .

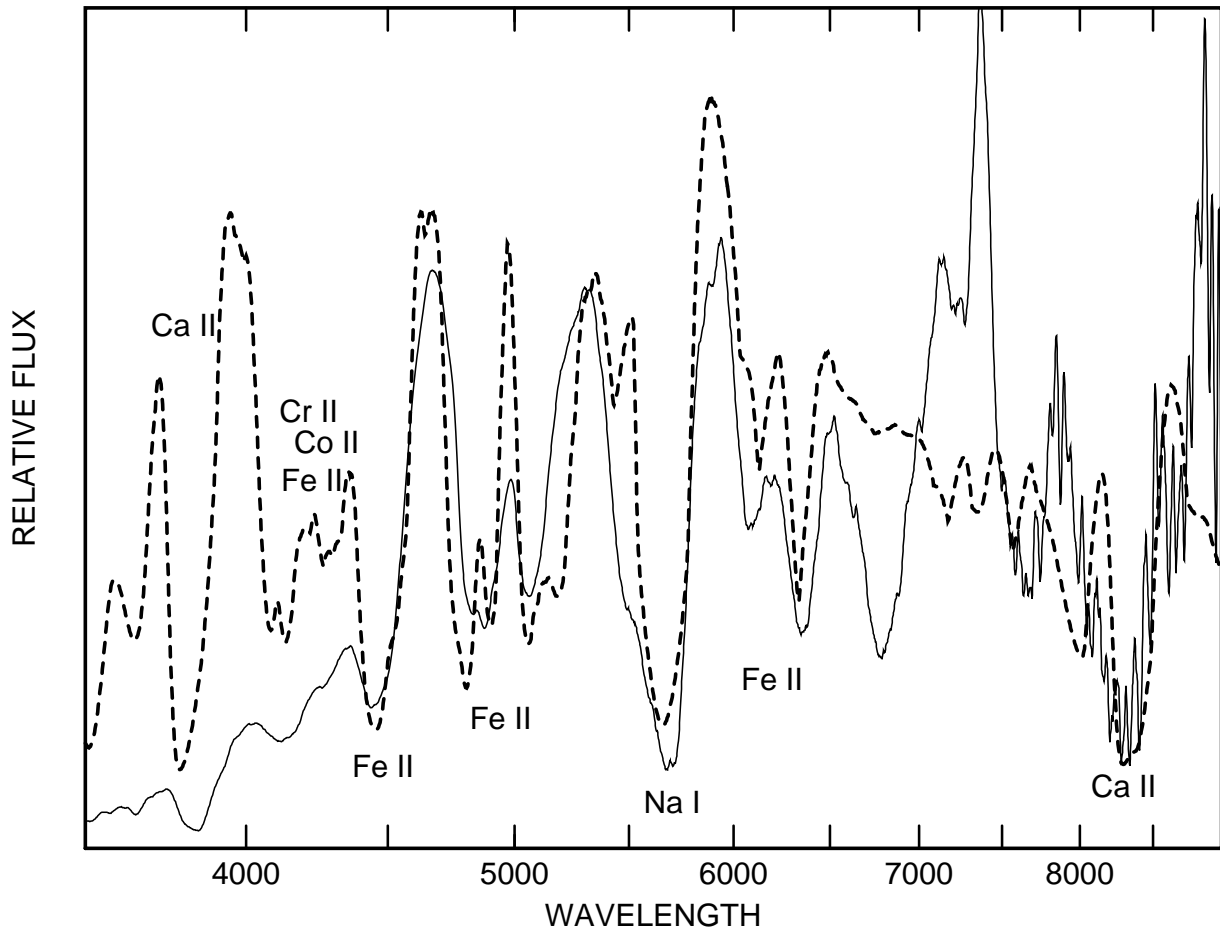


Fig. 10.— The day +115 spectrum of SN 1994D (*solid line*) is compared with a synthetic spectrum (*dashed line*) that has $v_{phot} = 6000 \text{ km s}^{-1}$, $T_{bb} = 15,000 \text{ K}$, and contains lines of four ions. The flux is per unit wavelength interval.

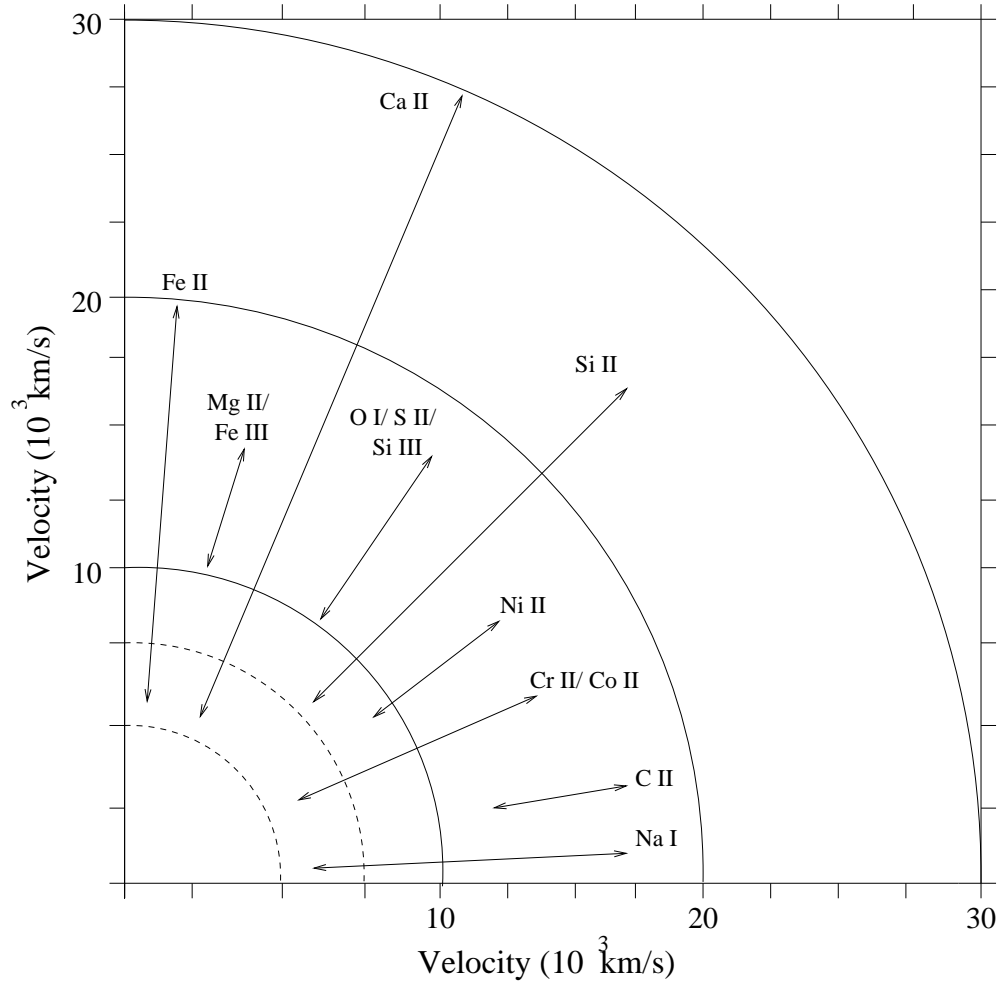


Fig. 11.— The velocity intervals within which the ions were used in the synthetic spectra. The upper bound is the velocity at which the line optical depth fell below 0.1.

Table 1. Input Parameters for SN 1994D

day	v_{phot} 10^3 km s^{-1}	T_{bb} K	v_e 10^3 km s^{-1}	T_{exc} K	τ C	τ II	τ O	τ I	τ Na	τ I	τ Mg	τ II	τ Si	τ II	τ Si	τ III	τ S	τ II	τ Ca	τ II	τ HV	τ Ca	τ II	τ Cr	τ II	τ Fe	τ II	τ Fe	τ III	τ Co	τ II	τ Ni	τ II	
-12	14	11	2	10	0.6	0.5	0.5	0	15	0.7	1	600	200	0	1.5	0	0	0	0	0	0	0	0	0	0	0	0	0	0	0	0	0		
-11	14	11	2	10	0.6	0.5	0	7	0.5	1	600	200	0	0.8	0	0	0	0	0	0	0	0	0	0	0	0	0	0	0	0	0	0		
-10	13	12	2	10	0.6	0.5	0	7	0.5	1	600	200	0	0.8	0	0	0	0	0	0	0	0	0	0	0	0	0	0	0	0	0	0		
-9	13	12	1	10	0.5	1	0.3	0.4	5	1	2	20	5	0	0.4	0.4	0	0	0	0	0	0	0	0	0	0	0	0	0	0	0	0		
-8	12	12	1	10	0.5	0.8	0.3	0.5	7	0.8	1.5	8	3	0	0	0.5	0	0	0	0	0	0	0	0	0	0	0	0	0	0	0	0		
-7	12	12	1	10	0.4	0.3	1	7	0.8	1.5				0	0	0.6	0	0	0	0	0	0	0	0	0	0	0	0	0	0	0	0		
-4	11	13	1	10	0.2	0.5	0	1	8	0.8	1.8	15	2	0	0	0.8	0.2	0	0	0	0	0	0	0	0	0	0	0	0	0	0	0		
-3	11	13	1	10	0	0.5	0.3	1	9	0.8	1.8	40	5	0	0	0.8	0.4	0	0	0	0	0	0	0	0	0	0	0	0	0	0	0		
-2	11	13	1	10	0	0.8	0.4	1	10	0.8	2	70	5	0	0	0.8	0.6	0.6	0	0	0	0	0	0	0	0	0	0	0	0	0	0		
-1	11	13	1	10	0	0.8	0.4	1	12	1.2	2	70	5	0	0	0.8	0.8	0.8	0	0	0	0	0	0	0	0	0	0	0	0	0	0		
2	11	35	1	10	0	2	0.15	1.5	12	0.8	2.5	70	2	0	0	0.8	0.5	0	0	0	0	0	0	0	0	0	0	0	0	0	0	0		
4	10	11	1	7	0	1.5	0.15	1.5	20	0.8	2	50	0	0	0.5	0.8	0.5	0	0	0	0	0	0	0	0	0	0	0	0	0	0	0		
5	10	14	1	7	0	0.3			15	0.8	1.5		0	0	1	0.8	1																	
7	10	14	1	7	0	0.8			10	1	1		0	0	2	1	5																	
10	10	12	1	7	0	2	1.5	0	10	0	1	10^3	0	1.5	4	0	10	8																
11	10	12	1	7	0	1	2	0	10	0	0.3×10^3	2×10^3	0	1.5	5	0	10	10																
12	10	12	1	7	0	1	1.5	0	8	0	0	2×10^3	0	2	6	0	12	15																
14	10	11	1	7	0	0	2	0	10	0	0	2×10^3	0	5	20	0	30	25																
15	10	9	1	7	0	0	1.5	0	10	0	0	2×10^3	0	5	50	0	30	15																
17	10	8	1	7	0	0	1.5	0	10	0	0	500	0	20	70	0	30	5																
19	9	8.5	1	7	0	0	1	0	6	0	0	500	0	40	100	0	40	0																
24	9	7.5	1	7	0	0	0.7	0	10	0	0	2×10^3	0	40	200	0	40	0																
28	9	7.5	1	7	0	0	0.7	0	10	0	0	2×10^3	0	40	200	0	40	0																
50	8	8	1	7	0	0	2	0	9	0	0	10^4	0	10	100	0	20	0																
87	6	8	1	7	0	0	10	0	0	0	0	10^4	0	5	50	0	10	0																
115	6	15	1	7	0	0	10	0	0	0	0	10^4	0	5	50	0	10	0																